CFD-SIMULATION AND EXPERIMENTAL VALIDATION OF HEAT TRANSFER IN LIQUID PISTON COMPRESSORS

Schober M.[a], Deichsel M.[a,*] and Schlücker E.[b]
*Author for correspondence
[a]Department of Mechanical and Building Services Engineering, Institute of Technology Georg Simon Ohm, Nuremberg, 90489, Germany
E-mail: michael.deichsel@th-nuernberg.de
[b] Institute of Process Machinery and Systems Engineering, Friedrich-Alexander-University Erlangen-Nürnberg (FAU), Cauerstraße 4, 91058 Erlangen, Germany

ABSTRACT

The liquid piston concept is suggested to improve the efficiency of compression and expansion steps in thermodynamic processes, due to near isothermal compression or expansion. Within the concept a liquid piston is utilized to compress or expand a gas, instead of a solid piston. The liquid piston has some advantages, like perfect sealing of low molecular gases, high efficiency and realization of discontinuously piston motion. The good sealing characteristics arise from the perfect adaption of a liquid to an arbitrarily shaped wall. In the same way the high efficiency stems from intensive heat transfer between the gas and its surroundings during the process, due to a low volume to surface ratio. In order to define design guidelines for a liquid piston compressor or expander prototype, extensive knowledge of the thermodynamic processes within the gas chamber are necessary. Therefore the heat transfer of a compression process with helium gas in tube bundle chamber geometry has been studied. The heat transfer is analyzed by a computational fluid dynamics (CFD) model, considering one tube with 38 mm in internal diameter and 2000 mm in length, at different compression times from 12 s to 60 s. The gas is compressed to 10 MPa, starting at 5 MPa and ambient temperatures about 293 K, with different pressure ratios around 2. In order to verify the computational model, the results are compared to measured experimental data from a testing device. The device compression chamber is equipped with a pressure transducer and several thermocouples in radial and vertical direction. The gas used in experiment is helium, while for the liquid piston hydraulic oil is applied. The results showed a good match in local temperature and pressure between the computational model and the experimental data. Based on these results the heat transfer coefficient was calculated for the different compression times, showing values from 153 W/m²K up to 252 W/m²K. These measures are leading to near isothermal compression, increasing the efficiency of any thermodynamic cycle with gas compression, the liquid piston concept is included. The liquid piston concept has several benefits due to compression and expansion process components, which makes it interesting for the Stirling cycle. Further investigations also will be done in using the liquid piston concept, respectively isotherm compression, in refrigeration cycles.

INTRODUCTION

Gas compression is an important part of many thermodynamic cycles. The system efficiency is mainly determined by the approach of isothermal behavior during the compression and/or the expansion process. An isothermal approach presupposes an intensive heat transfer between the gas and the chamber walls, which are tempered by a heat sink. In order to compress the gas, reciprocating compressors are widely used, but do have some shortcomings. Due to the compact design and high operation frequency, the surfaces for heat transfer are quite small, resulting in a rising gas temperature. This thermodynamic process is far from isothermal behaviour, but rather isentropic, decreasing the efficiency. Especially the compression of low molecular gases such as hydrogen or helium at high pressure generates a loss in efficiency either because of gas leakage or friction loss due to costly mechanical sealing methods.

The described shortcomings can be resolved by a liquid piston compressor. Within the liquid piston compressor, the solid piston is replaced by a liquid column to compress the gas in the working chamber. Since the liquid adapts perfectly to an arbitrarily shaped surface, it ensures perfect sealing of the working space to avoid leakage. This allows the use of many small pipes in a bundle, to maximize the heat transfer area. Through this method, the heat transfer between the gas and surrounding walls is supposed to be greatly improved, leading to near isothermal gas compression.

The first known use of the liquid piston was the Humphrey Pump, an internal combustion pump on Atkinson cycle with direct contact between the explosion and the water surface in a U-shaped tube, forcing the water to the upper level [1]. The Liquid piston concept combined with the Stirling cycle, and powered by solar energy, is particularly suitable for water pumping operations in structurally weak and rural areas [2,3]. The development of Fluidyne Stirling engine concentrates on performance improvements for pumping activities with direct connection between the pumping fluid and thermodynamic cycle [4-6]. The utilization of the liquid piston concept to improve heat transfer, reaching a near isothermal process, was not recognized. The liquid piston concept is then utilized firstly to improve the efficiency of gas compression and expansion in a tube bundle [7].

NOMENCLATURE

h	[W/(m²/K)]	Heat transfer coefficient
H	[J]	Enthalpy
κ	[-]	Heat capacity ratio
n	[-]	Polytropic index
p	[MPa]	Pressure
q	[W/m²]	Heat Flux
Q	[J]	Heat
T	[K]	Temperature
v	[m³/kg]	Specific volume
W	[J]	Work

Subscripts

isen	Isentropic
ith	Isothermal
pol	Polytropic

Within this work a simulation is developed to compare the efficiency of liquid piston and conventional reciprocating piston systems, while taking into account heat transfer and frictional forces. Based on these results, analytical studies are performed in order to obtain theoretical efficiency values and operational behaviour, due to a numerical model, simulating a single compression stroke [8].

The liquid piston technology is also widely discussed for the use in a Compressed Air Energy Storage (CAES) system. Some publications introduce the liquid piston in combination with CAES [9], giving a design scenario [10] and an initial experimental study [11]. The objective from both analytical and experimental work is to develop a powerful and efficient compression and expansion device for CAES. A research group utilizes spray cooling to improve heat transfer between gas and liquid piston spray [12]. It is followed by a theoretical investigation showing a design proposal for a multistage compression device for CAES, increasing the efficiency from 27.0% to 89.0% [13].In order to predict temperature and pressure curves of the gas compression, the process was modelled by numerical simulations, shown in several publications, for example in Ocean Compressed Air Energy Storage (OCAES) with a liquid piston in a cylindrical chamber [14]. Further in a tube bundle [15] or in a cylindrical chamber with different values in diameter and length [16]. The temperature and pressure curve was modeled after the isentropic exponent κ, as a significant result [16]. For the cases computed, it varies from 1.124 to 1.305.

The field of publications with numerical simulation is expanded by combined publication, including a numerical model and the experimental verification [17]. Efficiency is studied under the influence of piston velocity, displacement profile, compression ratio and chamber geometry. The analysis of a double step liquid piston compressor introduces some design factors for better verification [18]. Further on, a good comparison between theoretical analysis and experimental results is achieved [19]. This work was focused on the development of a temperature profile in a compression time range from 2.5 s to 40.0 s. A temperature difference of 73.0 K was achieved, with respect to the initial state. Additional publications utilize metal foam, inserted in the working chamber to increase the heat transfer area and to reduce the temperature rise during the compression process [20-22].

The above mentioned publications are studying the compression of air to low pressures up to 3 MPa, more related to CAES. This work focuses on heat transfer in a liquid piston compressor, as used in a Stirling cycle for example. Therefore, helium is used as the gas with a maximal pressure up to 16 MPa. The compression chamber has a cylindrical geometry representing one pipe of many in a tube bundle. Although the liquid piston can perform compression and expansion processes, only compression will be investigated in this study. To calculate the required quantities, CFD simulations with variations in chamber diameter and compression time are performed. In order to verify the computational results, experimental studies are carried out with exact documentation of pressure and local temperature in radial and vertical direction. The Liquid piston concept can be evaluated through the achieved heat transfer coefficient.

COMPRESSION THEORY

The necessary work of liquid piston compression is influenced by the thermodynamic process, including isothermal process, isentropic process and polytropic process under reversible conditions. **Figure 1** shows the compression process in an open system, including transferred heat and work.

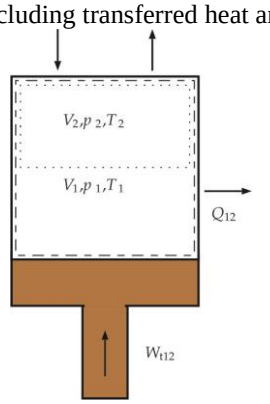

Figure 1: Compression process in an open system

In case of isothermal compression, work W_{12} supplied by the piston, is converted into heat Q_{12} and transferred completely to an external heat sink. The enthalpy remains constant (dH = 0) leading to no change in temperature ($T_1 = T_2 = T$). The Pressure endpoint p_2 can be calculated through the Boyle-Mariotte law ($p \cdot v$ = const.). The process can be regarded as an unattainable thermodynamic limit case, because heat transfer requires a temperature difference. The case is approximated in reality, by slow running machines. In the isentropic process the system boundary is isolated in a perfect way, not allowing heat transfer ($Q_{12} = 0$). Work input W_{12} is completely saved by the gas and therefor causes an increase in enthalpy. This increases temperature and pressure. The process can be characterized through the relation ($p \cdot v^{\kappa}$) with κ being the heat capacity ratio. The isentropic process represents the opposite thermodynamic limit case to the isothermal case. In reality the process almost occurs in very fast running reciprocating piston compressors with compact construction. In the polytropic case, work input W_{12} rises the enthalpy of the gas. Due to the adiabatic system boundary, a portion of the enthalpy is transferred to an external

heat sink as heat Q_{12}. The heat transfer does not take place completely in contrast to the isothermal case. Dependent on Q_{12} the gas temperature increases. The endpoints can be calculated with the polytropic index n throughout the relation ($p \cdot v^n$).

Figure 2 shows the pressure volume diagram of isothermal, isentropic and polytropic compression. The area between the curves and the p-axis, marks the necessary work W_{12} to compress the gas. Accordingly, the isentropic case has the highest necessary work and thus lowest efficiency, compared to the other cases. The isentropic process consumes a minimum of work, leading to highest efficiency. The red dashed line indicates the polytropic case with work and efficiency values between the two limits.

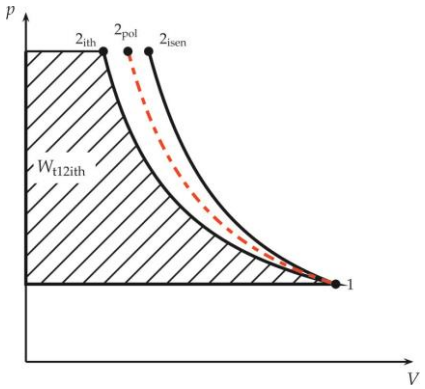

Figure 2: Pressure volume diagram of isothermal, isentropic and polytropic compression

NUMERICAL METHOD

In order to calculate the heat transfer coefficient between the gas and the wall, the gas condition during the compression process has to be known. Therefore, the commercial CFD-Code Ansys Fluent 15.0 is used. The simulation model includes only the volume of the gas, without wall thickness, assuming that the temperature change in the solid walls is negligible, compared to temperature change of the gas. In addition, the behaviour of the liquid piston is not the focus of this study, so it is neglected and its movement recreated by a moving boundary.

Since the flow of the problem is assumed to be axis symmetric, a two-dimensional axis symmetric model is created, shown in **Figure 3**. Axis r refers to radial direction and y to vertical direction. All boundaries in the model are stationary, except the bottom surface, representing the piston movement with a constant velocity in y-direction. A no-slip condition is applied on bottom, top and wall. The thermal boundary conditions are fixed to 293.2 K at the wall, and the top and adiabatic at the bottom. The Adiabatic condition is applied because of the used boundary moving strategy distorting heat transfer. Due to the existence of a small temperature difference in the lower part of the apparatus, the heat transfer is assumed to be negligible on this surface. The initial temperature of the gas is 293.2 K, and the initial pressure is 5 MPa.

The motion of the piston is realized through a motion profile calculating the current piston position from process time and constant piston velocity. To create the piston movement inside the domain, the dynamic layering technique is used. It removes layers of cells adjacent to the moving boundary, based on the height of the layer adjacent to the surface. Depending on an ideal cell height, the cells near the boundary are split or merged with the layer of cells next to it. In order to run the simulation a pressure-based solver with a segregated algorithm is used. Governing equations are calculated sequentially in a segregated manner. Gravity is included, and points in the opposite y-direction. In order to get experimentally comparable results, even at high pressure, a real gas model for helium is implemented, based on physical properties from the National Institute of Standards and Technology (NIST) database.

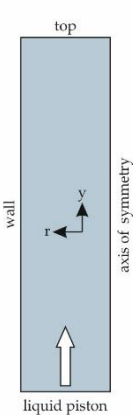

Figure 3: CFD-Model

For the pressure-velocity coupling, pressure implicit with splitting operators algorithm is chosen. For the spatial discretization of density, momentum and energy, a second order scheme is executed. The gradients for computing secondary diffusion terms and velocity derivatives at the cell centre are calculated by the Green-Gauss Node Based approach. For interpolating pressure the Pressure Staggering Option scheme is used. To calculate the transient problem a first order implicit method is performed. Iteration is stopped within each time step when all residuals are below 10^{-5} and energy is below 10^{-9}. The dimensions of the cylinder tube are 38 mm in diameter and 2,000 mm in height. The domain is meshed in a different manner, as shown in **Table 1**, to reach grid independence.

Table 1: Composition of analysed CFD grids

Grid	Element size in mm	Element direction	Element number		
	Centre	Wall	r	y	
1	2.0	0.20	24	1,015	24,360
2	1.4	0.14	35	1,443	50,505
3	1.0	0.10	49	2,015	98,735
4	0.7	0.07	70	2,872	201,040
5	0.5	0.05	98	4,015	393,470

All grids are structured using quadrilateral cells. The cell thickness in radial direction is small, near the wall, growing towards the centre. Centre cell and wall cell thickness is shown in **Table 1** and the ratio between is 10. In y-direction cell thickness has its minimum at the top, growing towards the bottom, with maximal thickness at this spot. The extreme sizes and the ratio between the two are equal to the discretization case in r-direction. To demonstrate grid independence a gas compression case with 12 s compression time is used. The gas flow is laminar at this compression time and the Reynolds number is 1,885 referring to the piston velocity. A suitable grid resolution is necessary at the boundary wall, to catch the transferred heat flux in a proper way. The results are showing a good approach of independent results, with growing grid refinement. The relative deviation between the heat flux from the gas to the wall of coarse (Grid 1) to fine grid (Grid 5) is

3.5%. According to the deviation between Grid 5 and Grid 2 of 2.0%, Grid 5 and Grid 3 of 1.0% and Grid 5 and Grid 4 of 0.3%, Grid 3 with a cell thickness of 1mm is chosen, assuming that 1.0% is an acceptable deviation.

In order to choose a suitable time step size for good temporal discretization, the analysed simulation case is divided by five different numbers of time steps ranging from 1,000 to 16,000. Number of time steps is doubled between the cases. The results show a deviation of 0.05% between the coarse and fine resolution. To minimize the computational effort 1,000 time steps are chosen for all cycle times. There have been additional studies to ensure time step independence, even for long cycle times up to 60 s with 1,000 time steps. The result shows time step independence in its entirety.

The correct function is initially tested by setting up an adiabatic simulation case with no heat transfer between the gas and the surroundings. In such a system the work input has to be stored in the gas, leading to a fast rise in temperature and pressure. Results can be easily verified by the analytical correlation $(p \cdot v^{\kappa}) = \text{const}$. The results showed a perfect match between the data, proving correct conservation of mass and energy.

EXPERIMENTAL VERIFICATION

In order to verify the numerical simulation model an experimental setup is designed. The key component of the experimental setup is the compression chamber containing helium gas and the liquid piston medium Unisyn OL 32. **Figure 4** shows a scheme of the experimental setup.

Compression Chamber (1) is a cylinder tube with equal dimensions, as described in the numerical method. The wall thickness is 5mm, made of stainless steel, withstanding 20 MPa pressure. The Compression Chamber is surrounded by an additional pipe with an annular gap, containing cooling water, supplied by the Cooling Circuit (5). The gas is inserted by a Filling Device (2). The liquid piston is driven by the hydraulic circuit filling and emptying the Compression Chamber. The key component of the hydraulic circuit is an Internal Gear Pump (7) delivering hydraulic oil out of a Tank (8). To drive the pump an electric motor (25) with rotational speed control and a Variable Frequency Drive is used. The pipe system is connected via cutting ring fittings and Metal Reinforced Hoses (10), protected against overpressure by a Security Valve (9). To prevent fluid back flow through the pump a Check Valve (11) is installed.

Based on this setup there are three states of liquid piston movement. In the case of complete standstill the Internal Gear Pump (7) delivers fluid over an opened solenoid Bypass Valve (12). A Filter (13) keeps the fluid clean and a Plate Heat Exchanger (14) removes the heating from pressure loss back in the Tank (7). In a case of excessive cooling the fluid is post heated in the Tank (7) by a Heating Element (17) and unified by a mixing device (MD) (18). The fluid is heated and cooled in a way that the temperature is equal to the wall temperature of 293.2K. In the filling case the liquid piston performs an upward motion. Therefore, the solenoid Filling Valve (19) is opened and all remaining valves are closed. When the level of the liquid piston reaches the Optoelectronic Level Switch (4) the filling time is started. The filling process is maintained until the filling time is equal to the user specified cycle time. At this point, the liquid piston has reached its Top Dead Center (TDC) and the gas compression is completed. In order to empty the Compression Chamber the Emptying Valve (20) is opened and the remaining valves are closed. To regulate the emptying time an adjustable Throttle Valve (21) is used, preventing the chamber from fast emptying because of high gas pressure. Through the throttle process the liquid is heated up and flows back to the Tank. To cool the liquid, it has to be pumped back through the cooling devices.

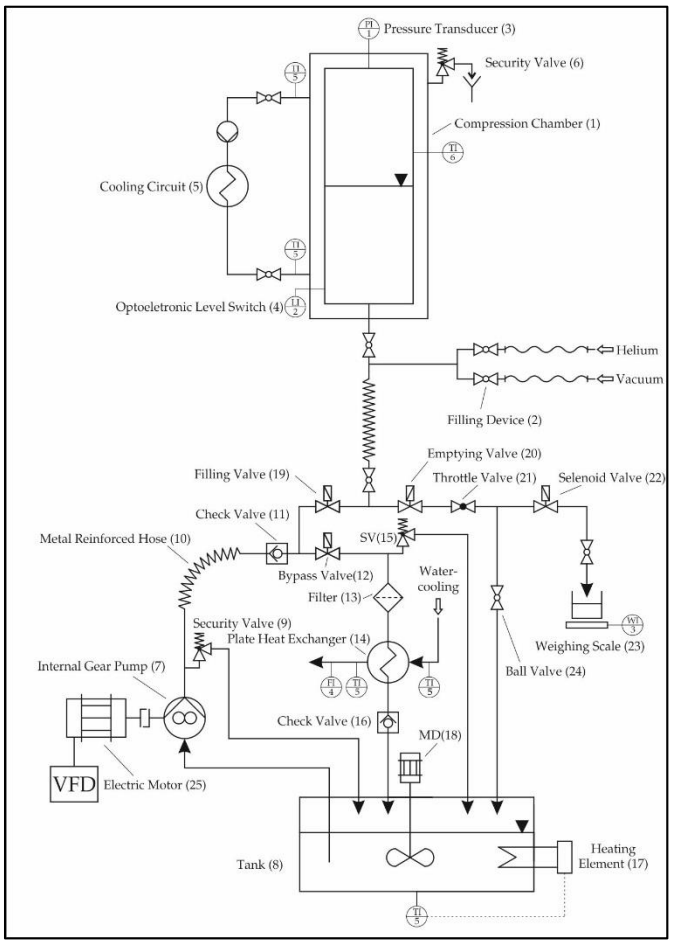

Figure 4: Experimental setup

The pressure of the working gas is measured by a Pressure Transducer, reaching to 16 MPa with a relative deviation of the full scale value of 0.05%. Manufacturer's data were checked by means of a deadweight tester. The volume of the gas, with the liquid piston in the upper dead position, was calculated by subtracting the volume of the liquid piston from the chamber volume. The liquid piston was weighed; redirecting the liquid piston flow during the emptying process to a Weighing Scale (23) by opening a Solenoid Valve (22) and closing a Ball Valve (24) in Tank direction.

The gas temperature was determined, by a Type K sheathed thermocouple with a sheath diameter of 0.05 mm and a wire diameter of 0.01 mm. In order to increase the response time, the thermocouple has an exposed probe tip located 2 mm from the

sheath end. To take into account response time and conduction losses, additional studies were performed. As a result from these investigations, a correction curve has been defined. Thermocouples were placed in different heights of the compression chamber. The thermocouple, for which the results are shown, is located at the centre of the compression chamber and in a height of 1,800 mm from the Bottom Dead Centre (BDC).

CFD-AND EXPERIMENTAL RESULTS

The results from the CFD-simulation are verified by experimental data as a basis for further studies. Therefore compression times of 12 s, 36 s and 60 s are investigated.

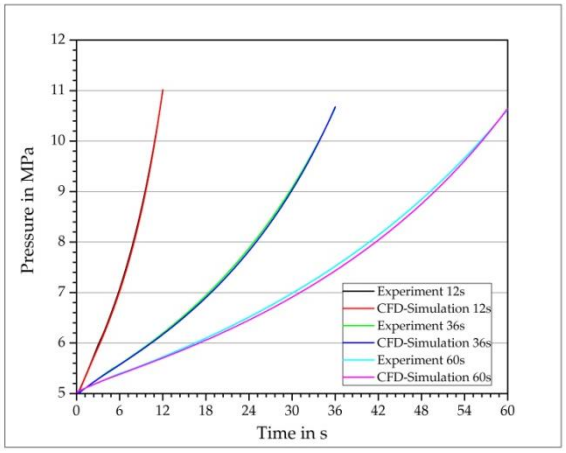

Figure 5: Experimental and CFD pressure curves

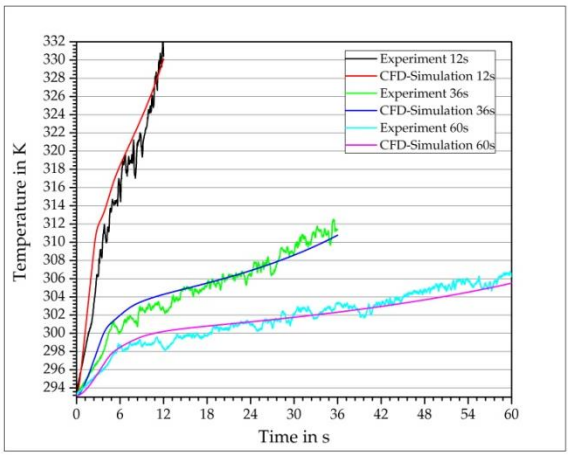

Figure 6: Experimental and CFD temperature curves

The constant liquid piston movement causes a linear decrease in the experimental gas volume and is well emulated by CFD-simulation. The pressure validation of the CFD-simulation is shown in **Figure 5**. It can be seen, that the data are in good arrangement within a relative deviation of 0.5%. From the experimental side, the pressure signal can be recorded without a time lag. **Figure 6** documents the verification process on gas temperature by comparing a sensor, located 1.800 mm from Bottom Dead Centre, in the centre of the compression chamber. Temperature in the CFD-simulation was calculated on location, identical to the sensor position in the experiment. The data are in good accordance but show a trend of better accordance with increasing time. The various curvatures of the graphs stem from compression time with different intensity in heat transfer and thus more steep or flat temperature graphs.

Figure 7 presents a velocity and temperature plot of the compression chamber at 36 s compression time. The fluid flow is upward at the centre with 0,08 m/s in maximum and downward at the wall with 0,03 m/s in maximum. The cooling effect of the walls is visible in the temperature plot.

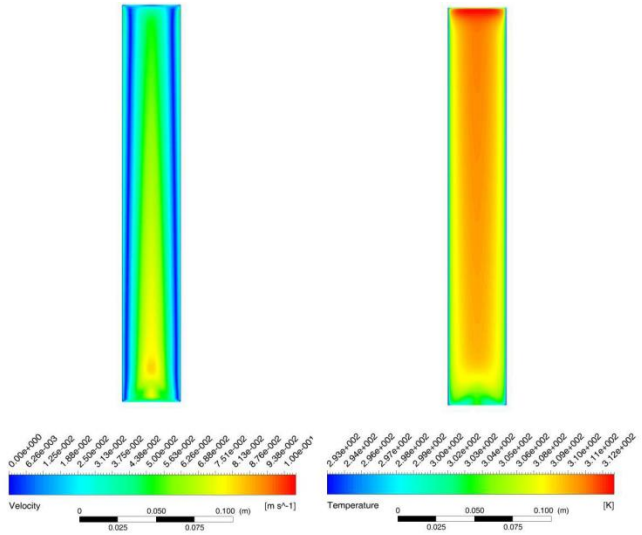

Figure 7: Final Velocity and Temperature plot at the 36 s case

HEAT TRANSFER CALCULATION

In order to determine the heat transfer coefficient between the wall and the gas, the experimental verified CFD-simulation is used. The heat transfer coefficient h can be expressed as

$$h = \frac{q_{wall}}{\left(T_{gas} - T_{wall}\right)} \qquad (1)$$

The heat flux at the wall q_{wall} is divided by the temperature difference between the current temperature of the gas and the wall temperature. The temperatures are volume averaged.

Figure 8 shows the heat transfer coefficient at the wall for different compression times. The averaged area values are very high at the beginning due to the small temperature difference between gas temperature and wall temperature. This indicates a mathematical phenomenon, because even without flow there is heat conduction. Considering the end of the compression process, a heat transfer coefficient of 252 W/(m^{2}K) is achieved, at 12 s compression time. In the middle of the analysed time frame at 30s, the calculation comes to a value of 183 W/(m^{2}K). Increasing the compression time to 60 s, the heat transfer coefficient drops to 153 W/(m^{2}K). The analysis shows smaller values for the heat transfer coefficient with increasing compression time. The reason for this is a less energetic velocity field, with decreasing compression time and thus a less intense contact between gas and wall.

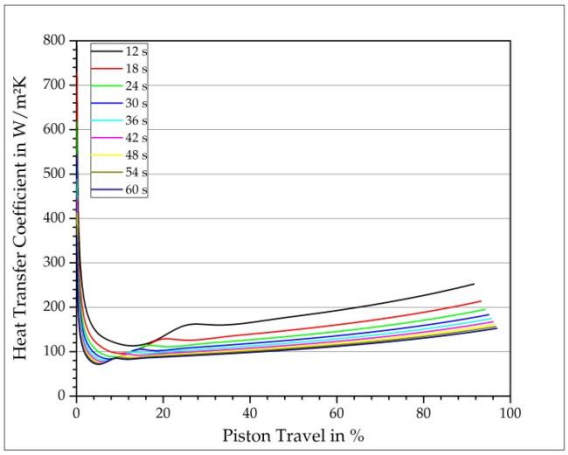

Figure 8: Heat Transfer Coefficient at the wall for different compression times

CONCLUSION

Liquid piston compressors can improve the efficiency of thermodynamic cycles, by approaching isothermal compression. The development of design guidelines necessitates a broad knowledge of the heat transfer mechanisms, occurring in the compression chamber, between the gas and the wall. Therefore a CFD simulation model was created, describing the heat transfer based on gas condition, during the compression process. The CFD simulation was verified by comparison of volume, pressure and local temperature curves of the simulation data and experimental results. The experimental values were measured at a testing device. After verification, the averaged area heat transfer coefficient between the gas and the wall was calculated from the temperature difference between the two locations and the heat flux at the wall. Analysing a compression time frame from 12s – 60 s, a maximal value of 252 W/(m^2K) was achieved at the end of the compression process and at 12 s compression time. The heat transfer coefficient decreased to 183 W/(m^2K) at 30 s and to 153 W/(m^2K) at 60 s compression time. The acquired knowledge of heat transfer allows an optimal design of liquid piston compressors for efficiency improvement.

REFERENCES

[1] Humphrey, H.A., An internal-combustion pump, and other applications of a new principle, *Proceedings of the Institution of Mechanical Engineers*, Vol. 77, 1909, pp. 1075-1200.

[2] Klüppel, R.P., Gurgel, J.M., Thermodynamic cycle of a liquid piston pump, *Renewable Energy*, Vol. 13, No. 2, 1998, pp. 261-268

[3] d. Klerk, G.B., Rallis, C.J., A solar powered, back to back, liquid piston stirling engine for water pumping, *Journal of Energy in South Africa*, Vol. 13, No. 2, 2002, pp. 36-42.

[4] Stammers, C.W., The operation of the fluidyne heat engine at low differential temperatures, *Journal of Sound and Vibration*, Vol. 63, No. 4, 1979, pp. 507-516.

[5] West, C.D., The fluidyne heat engine, *Electronics and Applied Physics Division, Atomic Energy Research Establishment*, 1971.

[6] West, C.D., Liquid piston stirling engines, Van Nostrand Reinhold, New York, 1983.

[7] van de Ven, J.D., Li, P.Y., Liquid piston gas compression, *Applied Energy*, Vol. 86, No. 10, 2009, pp. 2183-2191.

[8] Piya, C., Sircar, I., van de Ven, J.D., and Olinger, D.J., Numerical modeling of liquid piston gas compression, *ASME International Mechanical Engineering Congress and Exposition*, 2009, pp. 507-517.

[9] Lemofouet, S., Rufer, A., A hybrid energy storage system based on compressed air and supercapacitors with maximum efficiency point tracking (MEPT), *IEEE Transactions on Industrial Electronics*, Vol. 53, No. 4, 2006, pp. 1105-1115.

[10] Li, P.Y., Loth, E., Simon, T.W., van de Ven, J.D., and Crane, S.E., Compressed air energy storage for offshore wind turbines, 2011.

[11] Villela, D., Kasinathan, V.V., Valle, S.d., Alvarez, M., Frantziskonis, G., Deymier, P., and Muralidharan, K., Compressed-air energy storage systems for stand-alone off-grid photovoltaic modules, *Photovoltaic Specialists Conference (PVSC), 35th I.E.E.E.*, 2010, pp. 962-967.

[12] Qin, C., Loth, E., Li, P., Simon, T., van de Ven, J.D., Crane, S., and Pourmousa, A., Spray-cooling for wind-based compressed air energy storage, *11th International Energy Conversion Engineering Conference, Joint Propulsion Conferences, American Institute of Aeronautics and Astronautics*, 2013, pp. 1-11.

[13] Quin, C., Loth, E., Liquid piston compression with droplet heat transfer, *51th A.I.A.A. Aerospace Sciences Meeting, American Institute of Aeronautics and Astronautics*, 2013, pp. 1-24.

[14] Park, J.-k., Ro, P.I., Lim, S.D., Mazzoleni, A.P., and Quinlan, B., Analysis and optimization of a quasi-isothermal compression and expansion cycle for ocean compressed air energy storage (OCAES), *Oceans*, 2012, pp. 1-8.

[15] Zhang, C., Saadat, M., Li, P.Y., and Simon, T.W., Heat transfer in a long, thin tube section of an air compressor: An empirical correlation from CFD and a thermodynamic Modeling, *ASME 2012 International Mechanical Engineering Congress and Exposition*, 9 November, 2012, pp. 1601.

[16] Zhang, C., Simon, T.W., and Li, P.Y., Storage power and efficiency analysis based on CFD for air compressors used for compressed air energy storage, *ASME 2012 International Mechanical Engineering Congress and Exposition*, 9 November, 2012, pp. 1797.

[17] Mutlu, M., Kilic, M., Effects of piston speed, compression ratio and cylinder geometry on system performance of a liquid piston, *Thermal Science*, 2014, pp.146.

[18] Dolatabadi, A., Fabris, D., and Samara-Rubio, D., Isothermal efficiency of liquid piston compressors employed in comopressed air energy storage systems, *AMSE 2013 Fluids Engineering Division Summer Meeting*, 7 July, 2013, pp.1-8.

[19] Park, J.-k., Ro, P.I., He, X., and Mazzoleni, A.P., Analysis and proof-of-concept experiment of liquid-piston compression for ocean compressed air energy storage (OCAES) system, *Proceedings of the 2nd Marine Energy Technology Symposium*, 2014, pp. 1-8.

[20] Zhang, C., Wieberdink, J.H., Shirazi, F.A., Yan, B., Simon, T.W., and Li, P.Y., Numerical investigation of metal-foam filled liquid piston compressor using a two-energy equation formulation based on experimentally validated models, *ASME 2013 International Mechanical Engineering Congress and Exposition*, 2013, pp. 1-12.

[21] Zhang, C., Simon, T.W., and Li, P.Y., Optimization of the axial porosity distribution of porous inserts in a liquid-piston gas compression using a one-dimensional formulation, *ASME 2013 International Mechanical Engineering Congress and Exposition*, 2013, pp.1-10.

[22] Zhang, C., Yan, B., Wieberdink, J., Li, P.Y., van de Ven, J.D., Loth, E., and Simon, T.W., Thermal analysis of a compressor for application to compressed air energy storage, *Applied Thermal Engineering*, Vol. 73, No. 2, 2014, pp.1402-1411.